Effect of SiC and borosilicate glass particles on the corrosion and tribological behavior of AZ91D magnesium alloy after PEO process

Luca Pezzato, Luca Lorenzetti, Lavinia Tonelli, Giulia Bragaggia, Manuele Dabalà, Carla Martinib, Katya Brunelli

EFFECT OF SiC AND BOROSILICATE GLASS PARTICLES ON THE CORROSION AND TRIBOLOGICAL BEHAVIOUR OF AZ91D MAGNESIUM ALLOY AFTER PEO PROCESS

In: Surface & Coatings Technology 428 (2021) 127901

EFFECT OF SiC AND BOROSILICATE GLASS PARTICLES ON THE CORROSION AND TRIBOLOGICAL BEHAVIOUR OF AZ91D MAGNESIUM ALLOY AFTER PEO PROCESS

L. Pezzato[a], L. Lorenzetti[b], L.Tonelli[b], G. Bragaggia[c], M. Dabalà[a], C. Martini[b], K. Brunelli[a]*

[a] Department of Industrial Engineering, University of Padova, Via Marzolo 9, 35131 Padova, Italy

[b] Department of Industrial Engineering, University of Bologna, Viale del Risorgimento 4, 40136 Bologna, Italy

[c]Department of Chemical Sciences, University of Padua, Via Marzolo 1, 35131, Padova, Italy

[*]Corresponding author: Luca Pezzato, luca.pezzato@unipd.it, lucapezzato@virgilio.it, +39-0498275498, Via Marzolo 9, 35131, Padova, Italy

Abstract

In this work, Plasma Electrolytic Oxidation (PEO) coatings were produced on AZ91D Mg alloy, using as electrolyte an aqueous solution containing both silicates and phosphates. SiC particles, or borosilicate glass particles or a combination of them (SiC + borosilicate glass) were suspended into the electrolyte.

The PEO-treated samples were characterized through Scanning Electron Microscope (SEM) (both on the surface and in cross section), X-Ray Diffraction (XRD) and X-Ray Photoelectron Spectroscopy (XPS) in order to study the morphology, thickness, adhesion, structure and composition of the coating as well as particle distribution. The corrosion behavior was analyzed by potentiodynamic polarization and electrochemical impedance spectroscopy (EIS). The wear resistance was evaluated by dry sliding tests *vs.* AISI 52100 bearing steel (block-on-ring contact geometry).

The results showed that both SiC and borosilicate glass particles were incorporated into the PEO layers. Glass particles contributed to enhance corrosion resistance, whereas SiC particles decreased it. On the other hand, SiC particles improved the wear resistance (due to enhanced load support), leading to an increase of the friction coefficient (due to an increase of the abrasive component of friction). The best combination of properties was obtained with the addition of glass particles for 3 min treatment time. In this way, both the corrosion and wear resistance were increased, minimizing the detrimental effects of SiC particles on the corrosion properties and the friction coefficient.

Keywords: Plasma Electrolytic Oxidation, Magnesium, Corrosion, Wear, Particles

1.Introduction

In recent years, the use of lightweight metals, particularly of magnesium (Mg) and its alloys, has been gaining increasing importance for applications in various machinery and transportation system, especially in aerospace and automotive components. [1] Weight saving, afforded by the high strength-to-weight ratio of Mg alloys, offers obvious advantages such as the reduction of fuel consumption and CO_2 emission. AZ91D (9 wt% Al, 1 wt% Zn) is one of the leading Mg die casting alloys used in structural applications for automotive and light truck components, due to the combination of good mechanical and physical properties, excellent castability and satisfactory saltwater corrosion resistance, achieved by controlling the impurity level of Fe, Cu and Ni [2]. However, the range of applications for AZ91D could be widened by further improving corrosion resistance [3], and tribological behaviour, which suffers from a remarkable tendency to plastic deformation [4]. In order to increase wear and corrosion resistance of Mg alloys, several types of coatings and treatments have been developed, including laser alloying, thermal spray, electrochemical and electroless plating, vapor deposition coatings, chemical conversion and anodizing [5,6]. Among these surface treatments, Plasma Electrolytic Oxidation (PEO) is a very promising process that can enhance the corrosion and wear resistance by producing a relatively thick, dense and hard ceramic layer on Mg alloys. [7] The corrosion and wear resistance of the PEO-treated samples is strongly influenced by several process parameters such as: current density, voltage, treatment time and electrolyte composition. [8] The PEO-treated surfaces are generally characterized by improved corrosion and wear resistance [11] or possess particular functional properties such as antifouling [12] or fungicidal [13] properties. One of the characteristics of PEO coatings is the possibility to incorporate compounds and particles from the electrolyte, thanks to the mechanism of coating growth and, in detail, to the formation of micro-discharges on the surface during the treatment. [9] Considering the incorporation of particles suspended into the electrolyte, recently O'Hara *et al.* [10] stated that the main mechanism of incorporation is the sweeping of suspended particulate into active discharge sites immediately after plasma collapse. Hence, the particles are trapped into the discharge channels: the incorporation could occur due to inert or reactive incorporation depending by the chemical nature of the particles. Particles with high melting point (such as graphite, SiC and others) and also metallic particles are simply incorporated inertly into the PEO layer. Particles with low melting point (as for example clay particles) are instead reactively incorporated into the coating due to a rapid melting/solidification process, forming generally amorphous phases that can significantly modify the corrosion performance of the coating. [14]

The incorporation of different kind of particles into PEO coatings produced on Mg alloys has been widely studied in literature, also with comprehensive review works, such as the one of Fattah-alhosseini *et al.* [15]. The influence of micrometric SiC particles on the tribological properties of PEO coatings has been already studied in literature on Al alloys, for example in the work of Yang *et al.* [16]. However, in literature, only few works investigated the effects of the addition micrometric SiC particles on the wear resistance of PEO-treated Mg alloys. Yu *et al.* [17] and Vatan *et al.* [18] reported an improvement in the corrosion and wear resistance of PEO coated AZ31 alloy with the addition of SiC, but in form of nanoparticles. Only the work of Lu *et al.* [19] reported the effect of SiC micrometric particles on the PEO-coated AM50 alloy, evidencing that the presence of the particles reduces the wear rate, increases the friction coefficient and does not substantially modify the corrosion resistance. Regarding the addition of borosilicate glass particles, only one recent work of Asgari *et al.* [20] highlighted that the presence of glass particles permits to increase the corrosion resistance thank to pore sealing, due to the melting of glass particles during coating growth, but the influence of glass particles on tribological behavior was not investigated.

In the present work, borosilicate glass particles or/and SiC particles were added to the electrolyte for PEO process of AZ91 alloy with the aim of studying the effect of the incorporation of these particles on the corrosion and tribological behavior of the PEO coating. The results of the particles-reinforced PEO coatings were compared both with conventional PEO coating, as well as with the untreated AZ91D. Two PEO treatment times were studied, working with high current densities and short treatment times.

2. Experimental

2.1 Production of PEO coatings

AZ91D samples (nominal composition in Tab. 1) were used as substrate for PEO coatings.

***Tab.1** – Chemical composition of AZ91D magnesium alloy (wt%).*

Mg	Al	Zn	Si	Mn	Fe	Cu
90.8	8.5-9.5	0.45-0.90	0.35	0.18	0.014	0.003

Conventional metallographic techniques were employed to polish the samples before the PEO treatment, consisting of a grinding step with abrasive papers (500, 800, 1200 and 4000 grit) followed by a polishing step with cloths and diamond suspensions (6 μm and 1 μm). After polishing, the samples were degreased by ultrasonication in acetone. The PEO process was performed using a TDK-Lambda DC power supply of 400V/8A capacity, working in galvanostatic mode at the fixed current

density of 0.5 A/cm^2 and with two different treatment times, 1 minute and 3 minutes (high current densities and short treatment times). During the treatments, the substrate worked as anode and the cathode was a carbon steel mesh. An aqueous alkaline solution containing 50 g/L of Na_2SiO_3, 40 g/L of NaOH and 50 g/L of $Na_5P_3O_{10}$ was employed as electrolyte to produce the standard PEO samples. Both electrical parameters and composition of the base electrolyte were chosen on the basis of previous works of the authors [21]. To the base electrolyte was added 80 g/L (3.2% vol.) of borosilicate glass particles, or 10 g/L (0.3% vol.) of SiC particles (hexagonal crystal structure) or the combination of them (Tab.2). Moreover, also 1 g/L of $C_{12}H_{25}NaO_4S$ was added to the electrolyte, which was magnetically stirred and maintained at ambient temperature by a thermostatic bath during all the process. The quantity of particles was optimized in a preliminary work considering the higher amount that can be added preserving a good quality of the coating in terms of porosity and thickness. Both borosilicate glass and SiC particles were of micro-metric dimensions and angular shape, as shown by SEM images in Fig.1. Glass particles (Fig.1a) were characterized by quite uniform dimensions, whereas SiC particles (Fig.1b) had a wide range of dimensions.

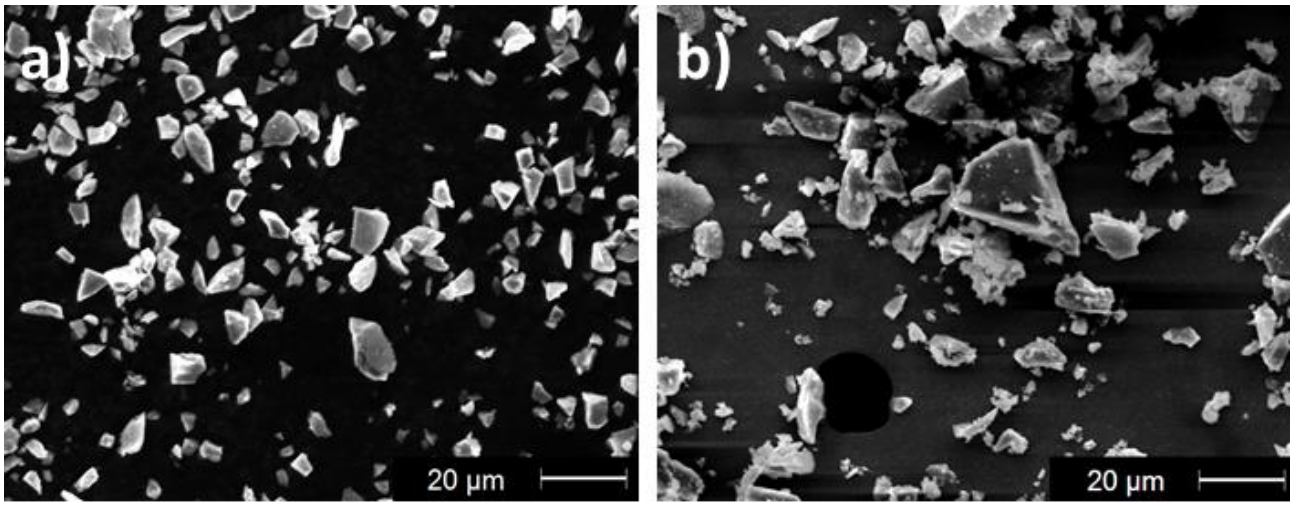

Fig.1 – *SEM images of SiC (a) and borosilicate glass (b) particles before incorporation in the PEO layers*

The different samples produced are summarized in Tab. 2.

Tab.2 – *Summary of the designation of the produced samples, obtained using in an aqueous alkaline solution containing 50 g/L of Na_2SiO_3, 40 g/L of NaOH and 50 g/L of $Na_5P_3O_{10}$ and a current density of 0.5 A/cm^2*

Name of the sample	Additives	Treatment Time (min)
PEO 1 min	-	1
PEO 3 min	-	3
PEO + SiC 1min	10 g/L SiC in 1 g/L $C_{12}H_{25}NaO_4S$	1
PEO + SiC 3 min	10 g/L SiC in 1 g/L $C_{12}H_{25}NaO_4S$	3
PEO + G 1 min	80 g/L Borosilicate Glass in 1g/L $C_{12}H_{25}NaO_4S$	1
PEO + G 3 min	80 g/L Borosilicate Glass in 1g/L $C_{12}H_{25}NaO_4S$	3
PEO + SiC + G 1 min	10 g/L SiC + 80 g/L Borosilicate Glass in 1g/L $C_{12}H_{25}NaO_4S$	1
PEO + SiC + G 3 min	10 g/L SiC + 80 g/L Borosilicate Glass in 1g/L $C_{12}H_{25}NaO_4S$	3

After the treatment the samples were washed with deionized water and dried with compressed air.

2.2 Microstructural and mechanical characterization

The cross sections of the PEO treated samples were cut, mounted in epoxy resin and polished. Both the surface and the cross section of the samples were analyzed with a Cambridge Stereoscan 440 scanning electron microscope, equipped with a Philips PV9800 EDS to evaluate composition, thickness, coating/substrate interface and microstructure of the coatings. In order to confirm the presence of the particles and to study their distribution, also EDS elemental mapping was performed. The phase analysis of the coatings was studied by a Siemens D500 X-ray diffractometer with a nickel-filtered Cu-Kα radiation source (λ = 0.15405 nm), operating at 40 kV and 30 mA (2θ range between 20° and 70° with a step size of 0.05 and counting time 5s). Identification of the phases was performed by the PDF-2 database.

XPS analyses were conducted through a Perkin-Elmer Φ5600ci spectrometer, with non-monochromatic Al radiation (1486.6 eV) at 250 W and a working pressure < 5 × 10-8 Pa. The binding energy (BE) of the Au4f7/2 line at 83.9 eV with respect to the Fermi level was assumed for the calibration. The standard deviation for the BE values was 0.15 eV. For the C1s line of carbon the BE value of 284.6 eV was assigned to correct the reported BE for the charging effects. [22]
Survey scans (187.85 pass energy, 1 eV/step, 25 ms per step) were obtained in the 0 - 1300 eV range. For the assignments of the peaks, after a Shirley type background subtraction [23], the NIST XPS

Database [25] and proper references [26-27] were employed. Deconvolution of the peaks was performed with XPSpeak 4.1 software.

The mechanical properties of the coatings were evaluated by Vickers micro-hardness tests, performed on polished cross section. The microhardness evaluation was carried out with a Vickers Leitz Wetzlar micro-hardness tester, using a normal load of 100 g.

Surface roughness of PEO layers was evaluated with a stylus profilometer (Hommelwerke T2000, 5 μm tip radius) by setting a measuring length Lt= 4 mm and a sampling length Lc=0.8 mm. Roughness parameters (Ra and Rq) were determined according to the ISO 4287 standard [28]. Coating practical adhesion was assessed by scratch tests (Revetest, CSM Instruments) using a Rockwell diamond indenter (200 μm tip radius). Scratch tests were performed with a progressive load from 1 to 30 N for a total length of 10 mm and with a linear speed rate of 10 mm min^{-1}.

2.3 Corrosion resistance evaluation

In order to evaluate the corrosion performance of the samples and the influence of the particles, potentiodynamic polarization (PDP) and electrochemical impedance spectroscopy (EIS) tests were performed. Also, untreated and PEO-treated samples without particles were tested as a reference for comparison.

An AMEL 2549 Potentiostat was employed for the electrochemical tests, performed in a 0.1 M Na_2SO_4 and 0.05 M NaCl solution, to simulate a moderate aggressive environment containing both sulphates and chlorides, in analogy with previous works of the authors on PEO coatings [21] Tests were performed using a saturated calomel electrode as reference (SCE) and a platinum electrode as counter. Potentiodynamic polarization tests were performed after 30 min of Open Circuit Potential (OCP) stabilization with a scan rate of 0.5 mV s^{-1} in a potential range from -2 to -0.6 V. Each measure was repeated three times in order to ensure the reproducibility of the test. Potentiodynamic polarization tests were performed only for a qualitative comparison of the behavior between the different samples, because no quantitative evaluation on the corrosion rate can be performed on samples coated with a thick insulating film, due to the fact that the Tafel law cannot be applied [21]. EIS tests were performed to quantitatively evaluate the corrosion performance of the samples. A Materials Instrument Spectrometer coupled with the 2549 Potentiostat was used for the EIS analysis, carried out at the open circuit potential in a frequency range between10^5 Hz-10^{-2} Hz with a perturbation amplitude of 10 mV. The experimental data were fitted with the software Z-view. Moreover, before the test the sample was immersed for 30 min for OCP stabilization and the measures were repeated three times to ensure reproducibility.

2.4 Tribological tests

The tribological behaviour of all PEO treated samples, with and without additives, was assessed by dry sliding tests performed at ambient conditions (50-60 % humidity and approx. 20 °C temperature). A block-on-ring configuration was adopted (ASTM G-77 [29]) using PEO treated flat sliders (5x5x70 mm^3) as stationary elements and a 100Cr6 (AISI 52100) bearing steel cylinder (40 mm diameter), with a 63 HRC hardness and R_a=0.09 μm surface roughness, as rotating element. Parameters for tribological tests were fixed at: 5 N normal load, 0.3 mm s^{-1} sliding speed, 500 m sliding distance. Test conditions led to a maximum and mean contact pressure of 44 and 34 MPa respectively, determined according to the Hertzian theory and assuming MgO as predominant phase for PEO layers (E=247 GPa and ν=0.187 [30]), as determined by XRD analyses. During tests, a bending load cell recorded the friction force and a linear variable differential displacement transducer (LVDT) registered the system wear (slider + cylinder) by assessing the vertical displacement of the slider. As a consequence, dynamic data of the coefficient of friction (COF) and system wear were recorded as a function of sliding wear. It is worth mentioning here that an increasing trend of system wear denotes material removal (i.e. wear) whilst a decreasing trend denotes material deposition (i.e. the formation of transfer layers). Vertical displacement data were used only to highlight possible wear transitions and correlate them with COF trends. Actual wear depth data were measured on sliders after the end of each test by a stylus profilometer (Hommelwerke T2000, tip radius: 5 μm), measuring at least three profiles on each wear scar (one in the centre and two at the sides). Wear depth values were then averaged again over the repetitions of each test.

Also dynamic COF values were averaged over the steady-state regime in each test and then over each repetition.

At the end of the tests, wear scar on sliders were observed by 3D-digital (Hirox KH 7700) and scanning electron (SEM, Zeiss EVO 50) microscopy to investigate wear mechanisms.

3. Results and Discussion

3.1 Microstructural and mechanical characterization

All the samples were observed by SEM both on the surface and in cross section. The results are reported in Fig. 2 for the samples obtained with 1 min treatment and in Fig. 3 for the samples obtained with 3 min treatment. The treated surfaces showed the typical morphology of PEO coatings on magnesium alloys, with the presence of pores, derived from the discharge phenomena, and pancake structures [31]. The values of thickness of coating, evaluated by SEM observation, and of the micro-

hardness, recorded in the cross section of the coatings, are reported in Tab. 3. An increase of the thickness with treatment time (from 1 to 3 minutes) for all the conditions (with and without particles) was observed, in agreement with literature [32]. The addition of borosilicate glass particles did not influence the thickness of the coating, whereas an increase of the thickness was observed for all samples containing SiC particles (Tab.3). This result is in accordance with the work of Wang *et al.* [33], regarding the effect of nano-SiC on the microstructure of MAO coatings formed on AZ91D alloy, and that ascribed this behavior to the electrophoretic effect of the SiC particles. In all the samples the coating resulted adherent to the substrate and quite uniform, whereas a rough surface was formed. Considering the presence of the particles, SiC particles were clearly observed on the surface and the cross sections of the samples treated for 1 min (Fig. 2c-d and 2g-h) and for 3 min (Fig. 3c-d and 3g-h), as highlighted by the white circles in the SEM micrographs. The particles exhibited the same shape and size of the original ones suspended in the electrolyte (Fig. 1a), indicating an inert incorporation into the coating. This is in accordance with results obtained by previous works on SiC-containing PEO coatings [34] and it is related to the melting point of SiC (about 2730 °C), higher than the temperature of arc plasma that, as evidenced by Lee *et al.* [35] ranges between 1800 and 2370 °C. Therefore, SiC particles cannot be melted during the PEO process and so they are simply incorporated into the coatings. The incorporation occurs thanks to the adsorption of the negatively-charged particles on the surface, followed by the entrance into the micro-discharge channels and molten material eruption that occurs during the process [15]. The inert incorporation of SiC particles was also confirmed by the high magnification observation of both the surface and cross section of the PEO + SiC + G sample, treated for 3 min (Fig.4). Both in the surface (Fig.4a, the white particles) and in cross section (Fig.4b, the particles evidenced by the white circles) the presence of the un-melted SiC particles with angular shape were noted. In detail, from the observation of the cross section (Fig.4b) the particles were present both into the pores and outside of the pores. The analysis of the surface (Fig.4a) evidenced also the presence of some defects (cracks) near the SiC particles.

The observation of the surface of the samples PEO with the addition borosilicate glass particles, obtained at 1 and 3 min, (Fig. 2e-g, Fig. 3e-g), showed that part of the pores was sealed. Therefore, a different mechanism was observed for the borosilicate glass particles in comparison with SiC particles. In the case of glass particles, their relatively low melting point (around 1650 °C) may produce a reactive incorporation of the particles into the coating. Specifically, the particles may rapidly melt and re-solidify, forming an amorphous phase that partially seals the characteristic pores of the PEO layer. Moreover, the obtained results are in accordance with Lu *et al.* [14], investigating other low-melting particles such as clay particles, and with Asgari *et al.* [20] reporting on another type of glass particles. In particular, accordingly to Asgari *et al.* [20], the collision of molten oxide

(formed in the micro-discharge holes during PEO treatment) with cold electrolyte leads to the solidification of molten glass and thereby forming pancake shape structures around micropores, with part of molten oxide that can return into the void and solidify producing a partial sealing of the pores. This is confirmed also by the high magnification observation of the cross section of the sample PEO + SiC + G (Fig.4b), where some pores, such as the one in the center of the image, resulted filled by the molten glass particles.

Micro-hardness data reported in Tab.3 showed that the addition of particles did not induce remarkable differences among the investigated PEO coatings and the measured $HV_{0.1}$ values were in accordance with the typical hardness of PEO coated magnesium alloys [36]. The coating hardness seemed to be more influenced by the modification of the coating induced by the particles (*i.e.* glass particles were beneficial for their pore sealing action) than by the intrinsic particle hardness (*i.e.* the hardest SiC particles did not allow to obtain the highest hardness values). The addition of SiC slightly reduced the average microhardness values (by about 10%), probably for the presence of defects (such as pores and cracks) at the particle/coating interface, due to inert incorporation of SiC, as observed in Fig.4a.

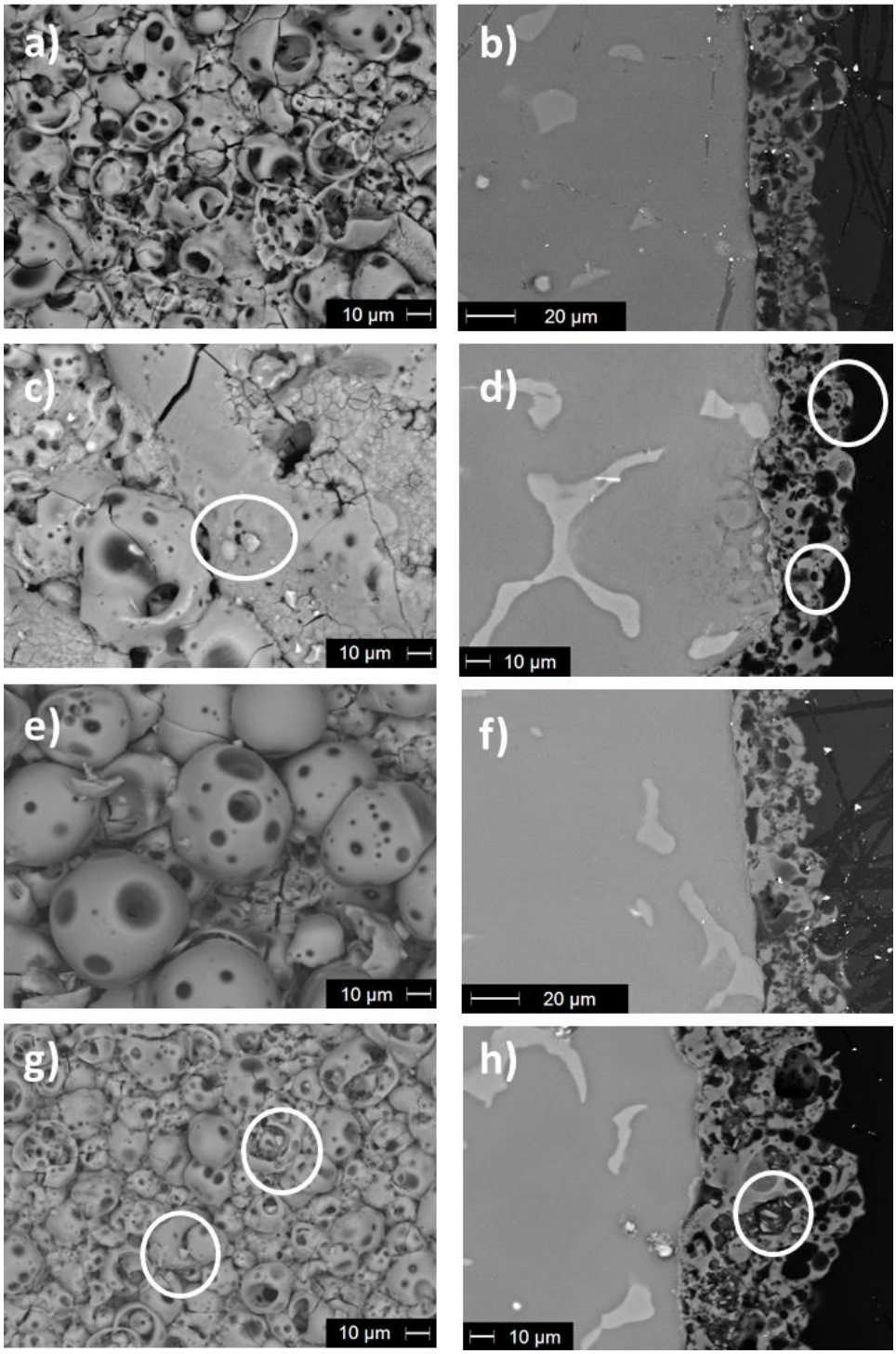

Fig.2 – *SEM images of the surfaces (left column) and cross sections (right column) of the samples obtained with 1 min treatment: PEO ((a) surface, (b) cross section); PEO + SiC ((c) surface, (d) cross section); PEO + G ((e) surface, (f) cross section); PEO + SiC + G ((g) surface, (h) cross section). The white circles indicate the position of SiC particles (when present).*

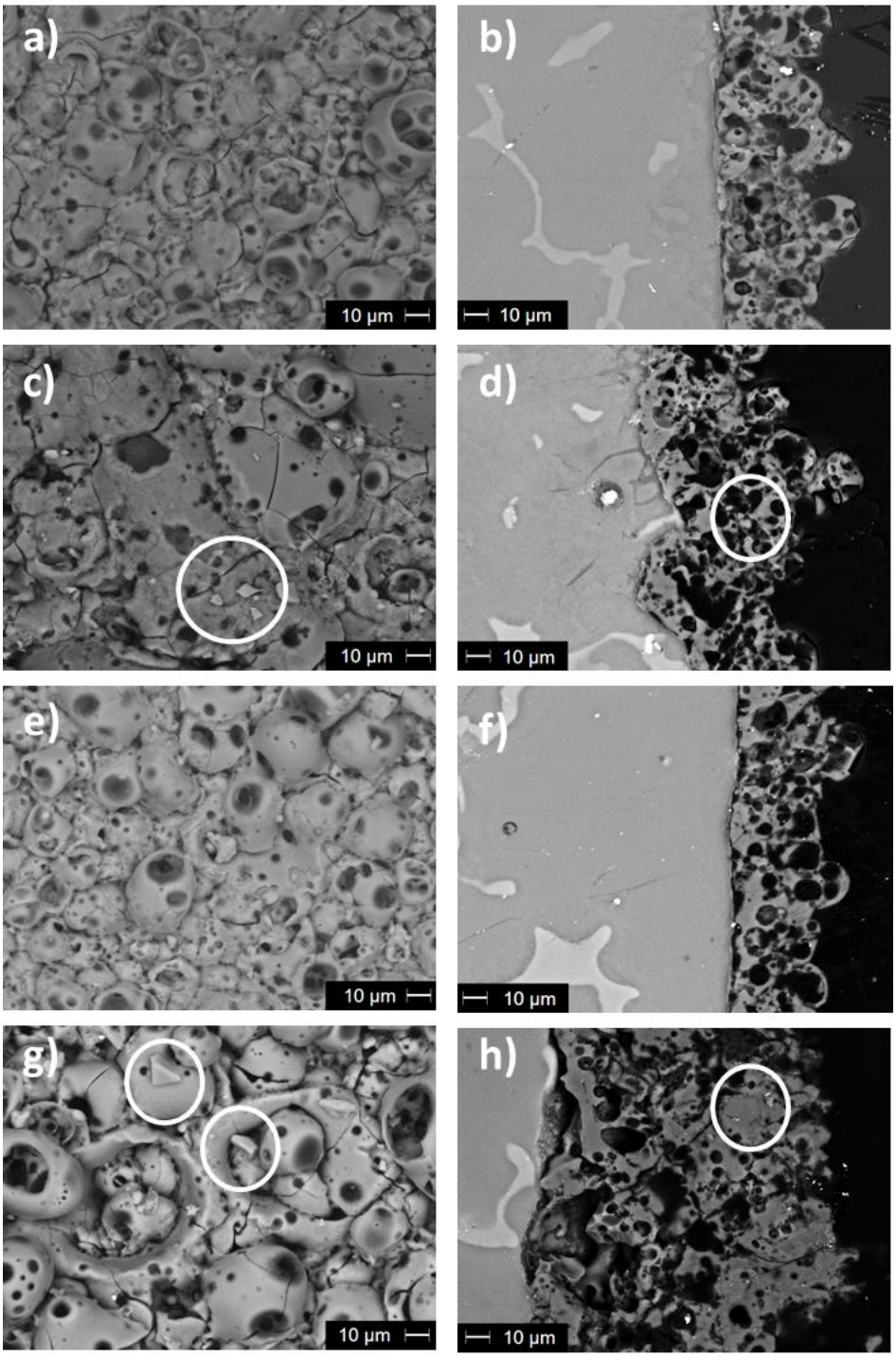

Fig.3 – *SEM images of the surfaces (left column) and cross sections (right column) of the samples obtained with 3 min treatment: PEO ((a) surface, (b) cross section); PEO + SiC ((c) surface, (d) cross section); PEO + G ((e) surface, (f) cross section); PEO + SiC + G ((g) surface, (h) cross section). The white circles indicate the position of SiC particles (when present).*

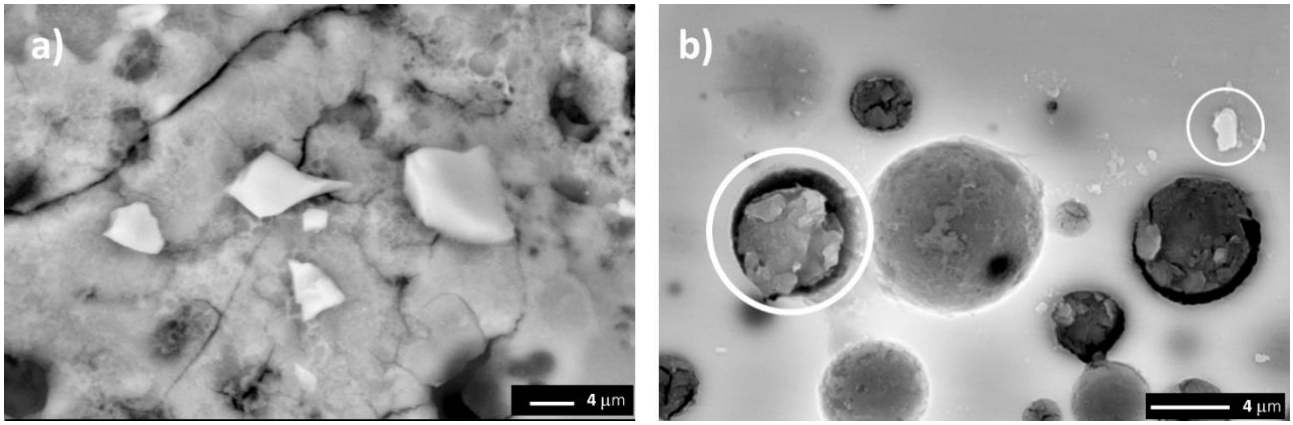

***Fig.4** – High magnification SEM images of the surface (a) and cross section (b) of the sample PEO + SiC + G obtained with 3 min treatment. The white circles indicate the position of SiC particles.*

***Tab.3** – Microhardness $HV_{0.1}$ and thickness of the PEO coatings*

Sample	1 min PEO	3 min PEO	1 min PEO + SiC	3 min PEO + SiC	1 min PEO + G	3 min PEO + G	1 min PEO + SiC + G	3 min PEO + SiC + G
Hardness $HV_{0.1}$	442 (± 20)	454 (± 30)	395 (± 20)	379 (± 15)	441 (± 10)	404 (± 15)	441 (± 10)	452 (± 15)
Thickness (µm)	29 (± 2)	47 (± 9)	33 (± 4)	58 (± 5)	32 (± 3)	42 (± 5)	53 (± 6)	97 (± 11)

Semi-quantitative EDS analysis were performed on extended areas of the cross sections of the different samples and the results are reported in Tab.4

***Tab.4** – EDS semi-quantitative results (wt%) obtained in the cross section of the different samples (extended area analyzed)*

	Mg%	Si%	P%	Al%	O%	Na%
PEO 1 min	22.57	16.35	8.45	2.58	36.63	13.42
PEO 3 min	24.48	16.63	7.97	2.54	38.60	9.79
PEO + G 1 min	21.78	19.38	8.02	1.62	38.27	10.94
PEO + G 3 min	20.23	19.86	9.09	2.25	39.68	8.89
PEO + SiC 1 min	22.12	17.97	10.12	2.01	38.45	9.33
PEO + SiC 3 min	24.02	17.82	12.14	2.31	35.08	8.64
PEO + SiC + G 1 min	19.58	20.95	9.92	2.01	38.66	8.88
PEO + SiC + G 3 min	17.33	21.19	8.57	1.96	38.62	12.33

It can be observed the presence of Al and Mg, coming from the substrate, and of Si, P and Na, coming from the electrolyte. The presence of Si can be related both to the sodium silicate in the electrolyte and to the addition of borosilicate glass and SiC powders. In fact, an increase in the silicon content in the samples obtained with powder addition was measured (about 3% for the glass particles and about

2% for SiC). No other significant trend was found for the other elements, that maintained more or less the same value in all samples, suggesting that the variation in the silicon amount is to be related to the particles addition and that an effective incorporation of both SiC and glass particles in PEO coating occurred.

In order to deeply study the elemental distribution, EDS elemental maps were performed on the surface and on the cross-section of the sample PEO with glass and SiC particles, produced with a treatment time of 3 min (PEO + SiC + G 3 min) and the results are reported in Fig. 5.

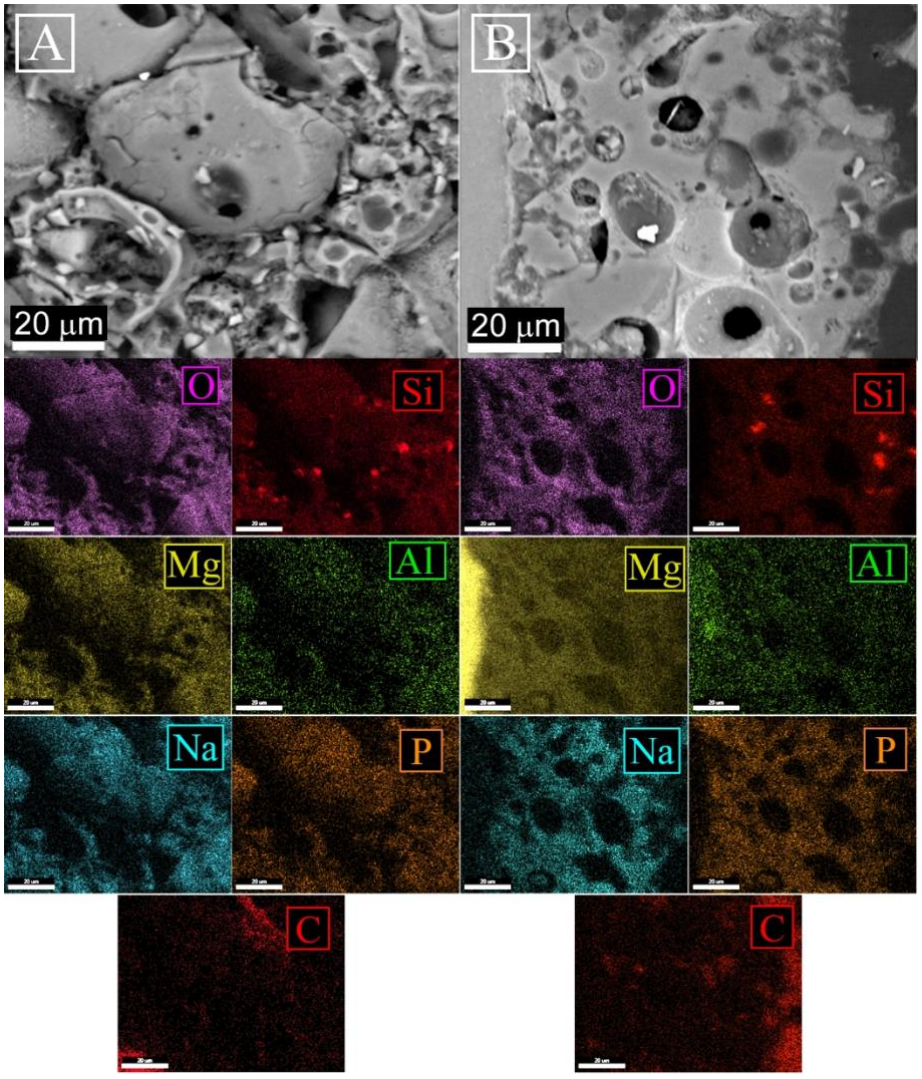

Fig.5 – *EDS elemental maps of the surface (a) and the cross section (b) of the sample PEO + SiC + G produced with a treatment time of 3 min*

X-ray EDS elemental maps showed a uniform distribution of the main elements that constituted the PEO layer, such as O, Mg, Al, P, Na and Si, and highlighted, both in the surface and in cross section, the direct incorporation of SiC particles. The particles were found both into the pores and incorporated into the coating.

Aiming at studying the phase structure of the different samples and to confirm the presence of the particles, XRD analyses were performed on all the samples and the results are reported in Fig. 6, for the samples treated for 1 min, and in Fig. 7, for the samples treated for 3 min.

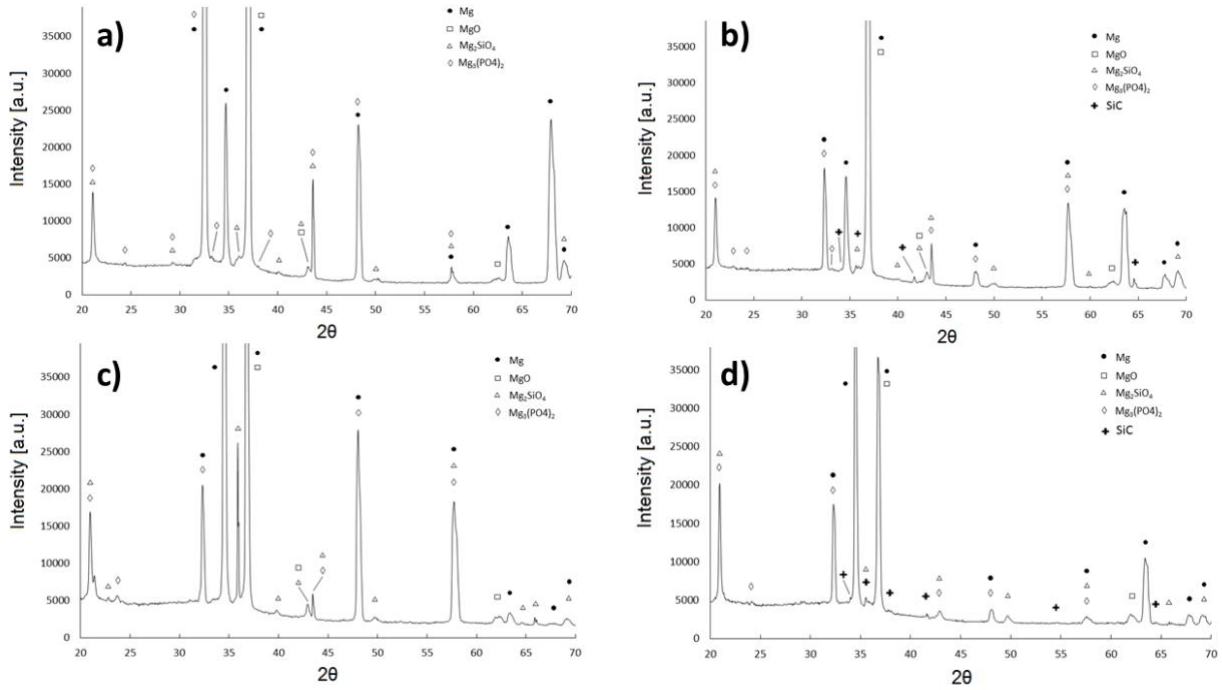

Fig.6 – *X-ray diffraction patterns of the PEO-treated samples (1 min of treatment time): PEO (a), PEO + SiC (b), PEO + G (c) and PEO + SiC + G (d)*

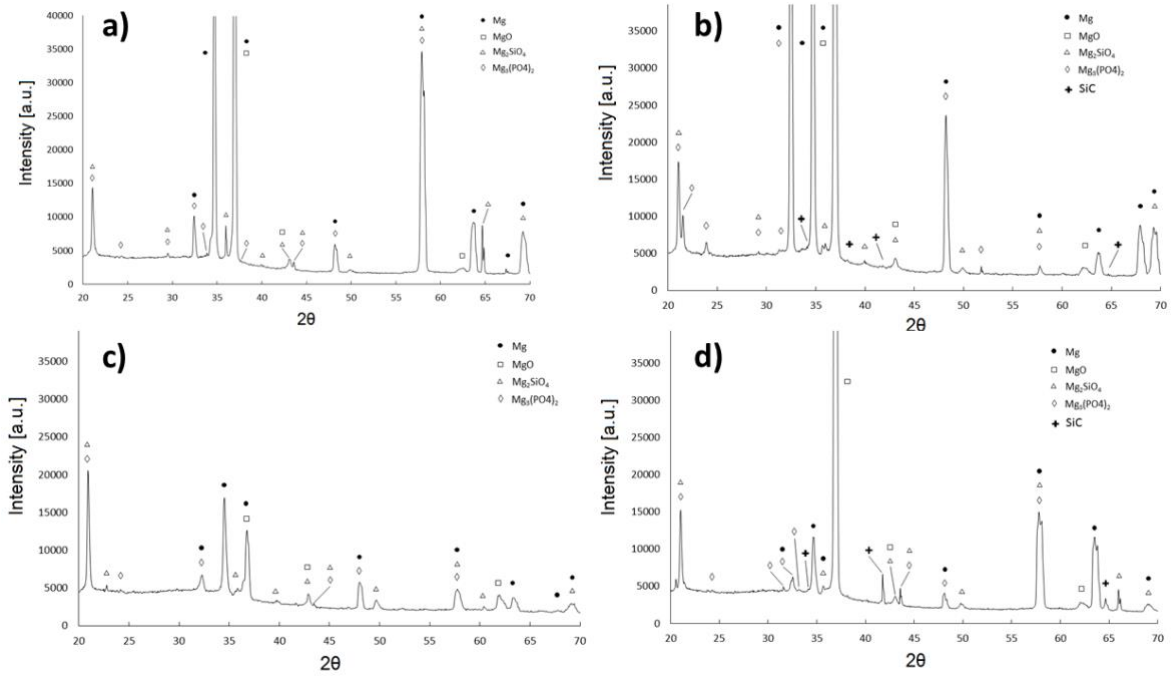

Fig.7 – *X-ray diffraction patterns of the PEO-treated samples (3 min of treatment time): PEO (a), PEO + SiC (b), PEO + G (c) and PEO + SiC + G (d)*

XRD analyses showed the presence of the peaks of Mg, due to the substrate contribution, and of MgO, Mg_2SiO_4 and $Mg_3(PO_4)_2$, indicating incorporation in the growing oxides of anions from the electrolyte (silicates and phosphates). This is in accordance both with previous work of the authors [21] and with the literature regarding PEO coatings [37-38] and is due to the interaction of chemical species into the discharge channels formed during PEO process.

In detail, as evidenced by Barati Darband *et al.* [32] in PEO processes, the magnesium substrate is placed as anode in basic electrolytes; thus, magnesium dissolution reaction occurs under a strong electric field producing magnesium ions accordingly to Eq.1

$$Mg \rightarrow Mg^{2+} + 2e^- \quad (1)$$

After the formation of magnesium ions, the different compounds are formed following the subsequent chemical reactions: MgO (Eq.2 and 3), Mg_2SiO_4 (Eq.4, thank to presence of SiO_3^{2-} ions coming from the electrolyte) and $Mg_3(PO_4)_2$ (Eq.5, thanks to the presence of PO_4^3 ions coming from the electrolyte).

$$Mg^{2+} + 2OH^- \rightarrow Mg(OH)_2 \quad (2)$$

$$Mg(OH)_2 \rightarrow MgO + H_2O \quad (3)$$

$$2Mg^{2+} + SiO_3^{2-} + 2OH^- \rightarrow Mg_2SiO_4 + H_2O \quad (4)$$

$$3Mg^{2+} + 2PO_4^{3-} \rightarrow Mg_3(PO_4)_2 \quad (5)$$

Moreover, in all the samples produced with SiC particles in the electrolyte (Fig. 6b and 6d for the treatment at 1 min, Fig. 7b and 7d for the treatment at 3 min) the peaks corresponding to SiC are visible, confirming the presence of this particles into the PEO layer. As expected, borosilicate glass was not detected by XRD analysis, due to its amorphous nature.

In order to investigate the surface composition of the samples, a XPS analysis on the bare surface (without sputtering) was carried out on the sample PEO + SiC + G with 3 min of treatment time: the resulting survey spectrum is shown in Fig. 8.

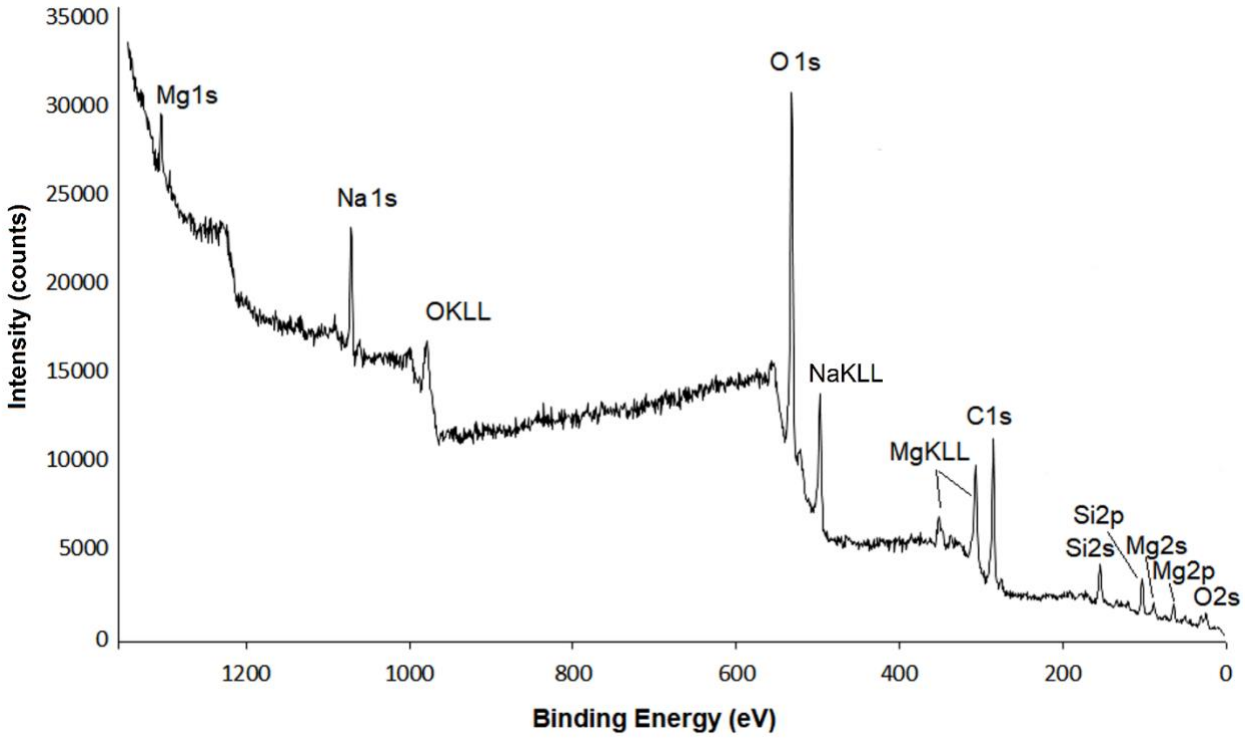

***Fig.8** – Survey scans collected from the sample PEO + SiC + G (3min of treatment time). Binding energies not corrected for surface charging. Minor and less visible peaks were not indexed*

The atomic percentages of the elements present on the surface of the coating were determined by the single XPS regions present in the survey and are reported in Tab. 5. The presence of C is due to adventitious contamination, and was used for referencing purposes to correct for charging effects.

***Tab.5** – XPS quantitative results (at%) of elements constituting the surface of the sample PEO + SiC + G (3 min treatment)*

C 1s	O 1s	Na 2s	Mg 2p	Al 2s	Si 2p	P 2p
26.0 %	47.9 %	9.1 %	3.1 %	2.8 %	9.4 %	1.7 %

The high-resolution Si 2p peak, reported in Fig. 9a, consists of three peaks: one situated at ~101.8 eV, attributed to silicon within the α-Mg_2SiO_4, a second located at ~102.9 eV, ascribable to γ-Mg_2SiO_4 [26], whereas the one at ~103.6 eV is related to the silicon within the SiO_2. [39]

The high-resolution peak of Mg 2p is shown in Fig. 9b. This peak can be deconvoluted into three main components: the one at ~49.6 eV corresponding to the magnesium within the $Mg(OH)_2$, the one at ~50.4 eV BE corresponding to $MgAl_2O_4$ and/or MgO, whereas the last at ~51.6 eV to the Mg_2SiO_4 and/or $Mg_3(PO_4)_2$. [24, 39]

The high-resolution P 2p peak, shown in Fig. 9c, resulted from the contribution of the peak at 133.1 and the one at 134 eV, corresponding to P $2p_{3/2}$ and P $2p_{1/2}$, respectively, and indicating the presence of $(PO_4)^{3-}$ species. These values can be attributed to the presence of $Mg_3(PO_4)_2$ and/or Na_3PO_4 [27].

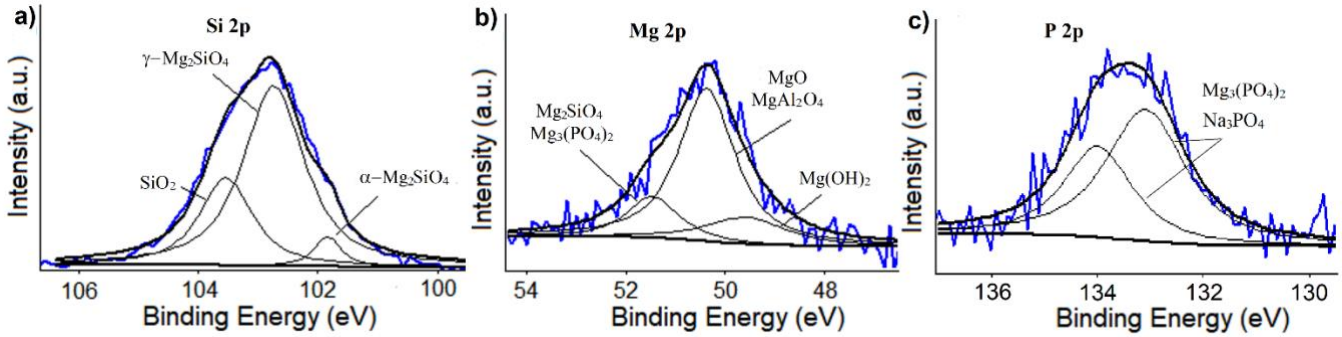

Fig.9 – *High resolution single peak spectra of the Si2p (a), Mg2p (b) and P2p (c) regions for the sample PEO + SiC + G treated for 3 minutes.*

Surface roughness data, reported in Fig.10, confirmed the observations on PEO coating morphology so far discussed. For 1 min treatment time, roughness was comparable for all PEO coatings, with Ra of about 4 µm. By increasing the treatment time to 3 min, the roughness of all coatings increased. The increase of surface roughness with treatment time for PEO layers is well-documented in the literature [32, 40]. As already mentioned, longer treatment time induces an increase in the layer thickness and, concurrently, the number or discharge channels decreases and their diameter increases. As a consequence, larger defects and discontinuities are formed, leading to a higher surface roughness. However, some differences can be observed among the 3 min coatings. In particular, PEO + SiC exhibited the highest roughness, while PEO layers with borosilicate glass particles (PEO + G and PEO + SiC + G) were characterized by the lowest roughness. In accordance to microstructural analyses, the higher surface roughness of PEO + SiC is presumably due to the presence of un-melted sharp SiC particles embedded in the coatings. On the other hand, the low surface roughness of PEO + G and PEO + SiC + G coatings can be related to the sealing tendency of the borosilicate glass, that reduced surface irregularities also in case of SiC addition.

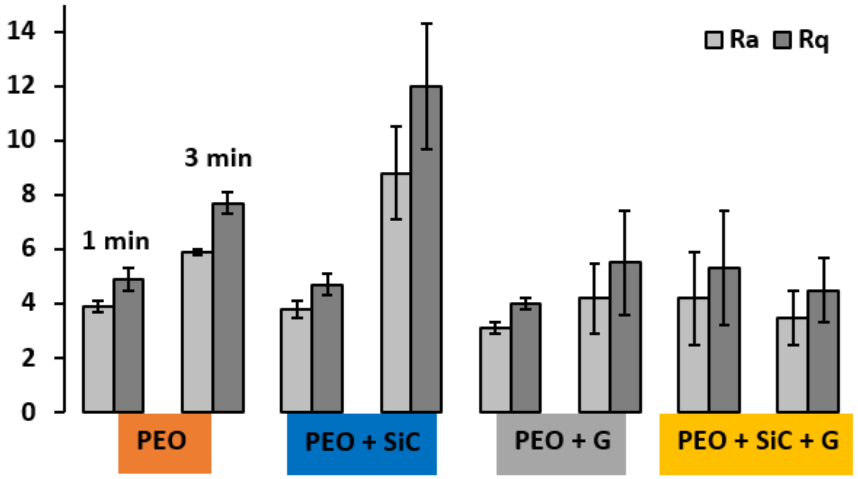

Fig. 10 *– Surface roughness parameters (Ra and Rq, according to ISO 4287) for the PEO coatings.*

The evaluation of practical adhesion of coatings is reported in Fig.11, where the critical loads obtained by scratch tests (in terms of Lc3, defined by ISO 20502 as: penetration of the coating to the substrate at the centre of the track [41]) are compared. Representative scratch plots and micrographs (both OM and SEM) for Lc3 identification are available in the supplementary material (Fig. S1). As observed in a previous work on PEO-treated EV31A Mg alloy [42], PEO layers plastically deform as they are bent into the track generated by plastic deformation of the substrate. On increasing normal load, buckling failures (cracks and patches of coating detachment) may appear within the scratch track. In this case, a few cracks appear at the edges of the scratch track, only for glass-containing PEO layers produced with 1 min treatments, probably due the pore-sealing action of glass which might reduce the strain tolerance of the oxide layers [43].

The Lc3 values ranged between 15.5 and 25.5 N for all PEO coatings. At both treatment time, the PEO layer without added particles exhibited a slightly lower adhesion than PEO layers with particles. Furthermore, an increase in the practical adhesion of all coatings was observed after the 3 min treatments, especially in case of particle additions. The Lc3 increase can be ascribed to increased layer thickness due to the longer treatment time. PEO + SiC and PEO + SiC + G obtained with the 3 min treatment were characterized by a slightly higher adhesion, presumably as a consequence of the presence of SiC particles which increased the load bearing capacity of the coating, as observed for other composite coatings [44].

It is worth noticing that PEO + G coating, at both 1 and 3 treatment time, showed the lowest standard deviation. This result is likely related to the sealing effect of borosilicate glass particles that led, as already discussed, to a lower surface roughness.

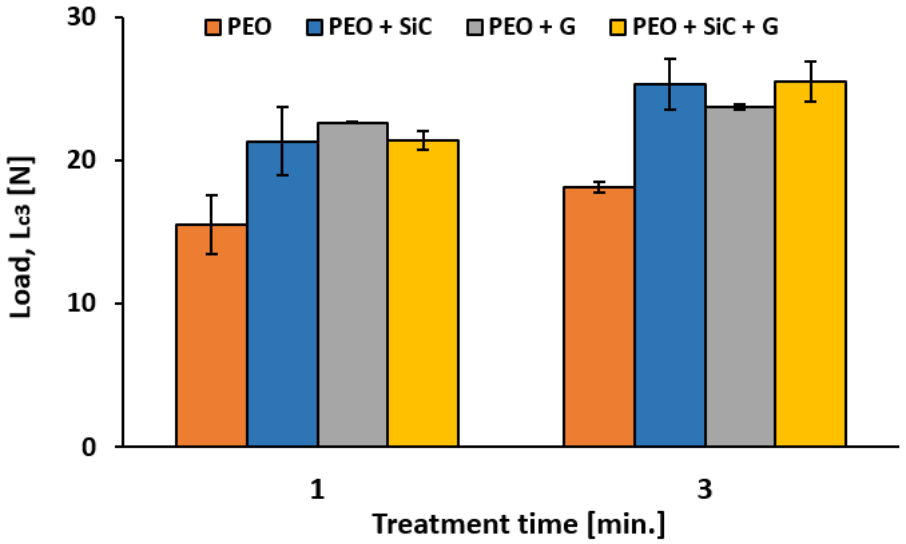

***Fig. 11** – Progressive load scratch test: L_{c3} values of scratch tracks of PEO treated samples: PEO, PEO + SiC, PEO + G and PEO + SiC + G.*

3.2 Corrosion Resistance evaluation

In order to qualitatively and comparatively analyze the corrosion properties of the PEO coatings produced with or without the addition of SiC or borosilicate glass particles, potentiodynamic polarization (PDP) tests were performed. The results are reported in Fig. 12a for the samples obtained at 1 min of treatment time and in Fig. 12b for the samples obtained at 3 min.

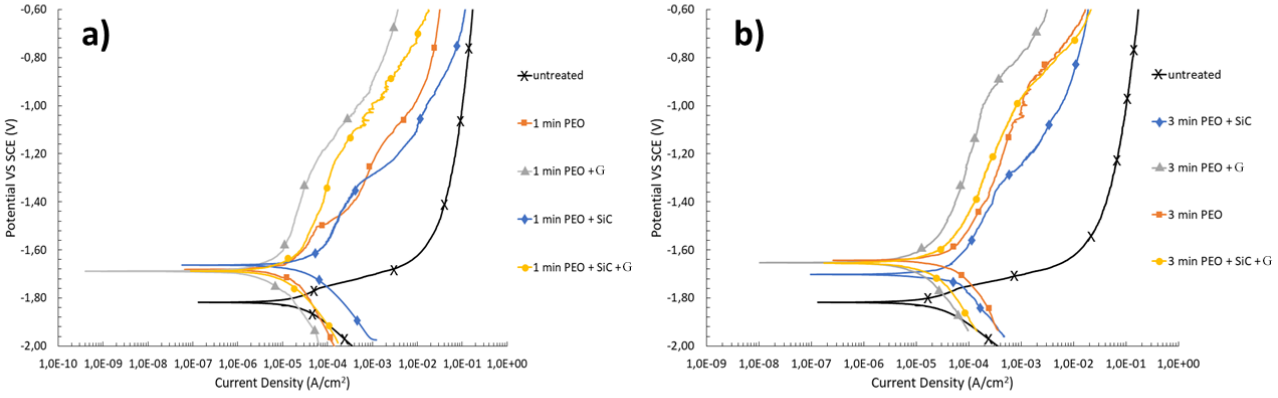

***Fig.12** – Potentiodynamic polarization curves of the PEO-treated samples. (a) Samples obtained with 1 min of treatment time; (b) Samples obtained with 3 min of treatment time. In both cases the results were compared with the untreated sample. (Test electrolyte: 0.1 M Na_2SO_4 and 0.05 M NaCl; SCE reference electrode)*

The PDP curves first of all show that all the PEO-coated samples exhibited improved corrosion performance in comparison with the untreated magnesium alloys, with a shift of the curves towards more noble potential and smaller current densities. Considering the PEO-treated samples with and without the addition of particles, no significant differences in the corrosion potentials were observed. Considering the currents, a shift towards lower current densities was observed for the samples containing glass particles (PEO + G and PEO + SiC + G), in comparison with the sample containing only SiC (PEO + SiC). However, due to the thick insulating nature of PEO coatings, the Tafel law cannot be applied and quantitative evaluation, such as calculation of the corrosion current and the corrosion rate, is not possible from PDP tests. Considering the anodic branch of the curves it can be observed a clear shift toward more negative currents for the PEO treated samples. Also, a shape change can be noted: the untreated sample in fact did not exhibit any passivation phenomena whereas a passive region can be identified for all the PEO treated samples, in particular in the sample PEO + G (both at 1 and 3 min of treatment time) that, therefore, can be considered the more promising in terms of corrosion resistance.

In order to quantitatively evaluate the corrosion performance of the samples and to study the effect of particles addition on the corrosion resistance, EIS tests were performed in the same electrolyte employed in PDP tests. The results in term of Nyquist plot are reported in Fig. 13, where dots represent the experimental data. The data from EIS tests were also fitted using the circuit reported in Fig. 14 and the results of the fitting, that are graphically represented in Fig. 13 as dashed lines, can be found in Tab. 6. The choice of the equivalent circuit was performed on the basis of the literature on PEO coatings [21] that suggests to employ a double circuit (Fig. 14b) to fit data coming from PEO treated samples in order to consider the presence of an inner and an external layer. The data coming from the untreated sample were instead fitted with a single circuit (Fig. 14a) because only the natural oxide layer is present on the surface. A good fitting quality was obtained, as confirmed by the low values of chi-squared in Tab. 6 and by the good correspondence between dots and lines in Fig. 13.

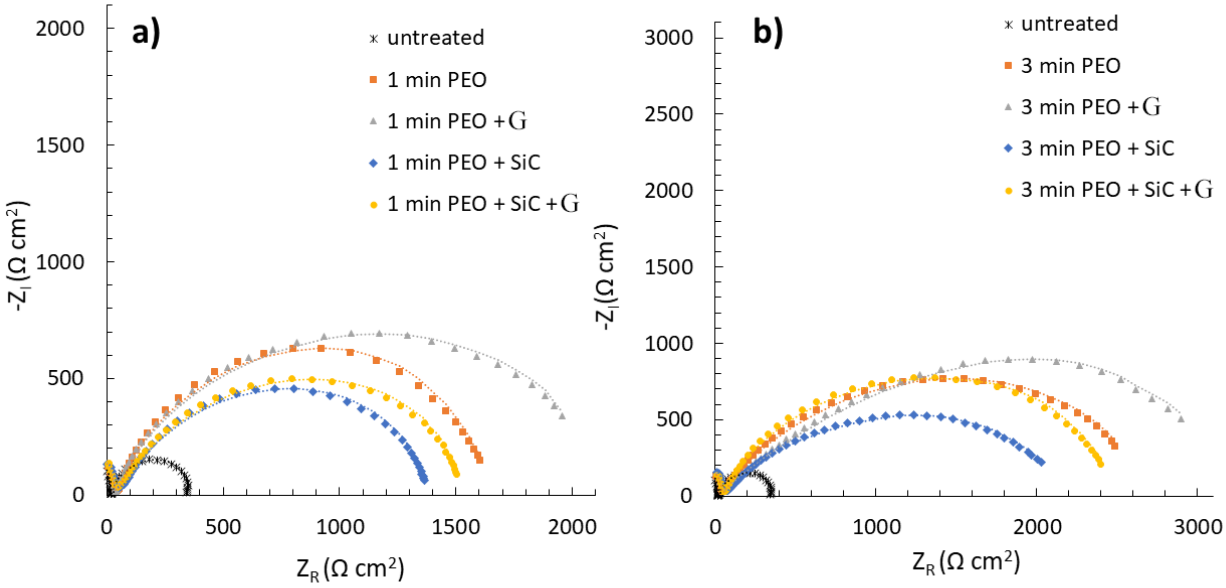

Fig.13 *– Results of EIS tests in term of Nyquist plots for the PEO-treated samples. (a) Samples obtained with 1 min of treatment time; (b) Samples obtained with 3 min of treatment time. In both the cases the results were compared with the untreated sample. (Test electrolyte: 0.1 M Na_2SO_4 and 0.05 M NaCl). Dots represent experimental data and dashed lines the result of the fitting.*

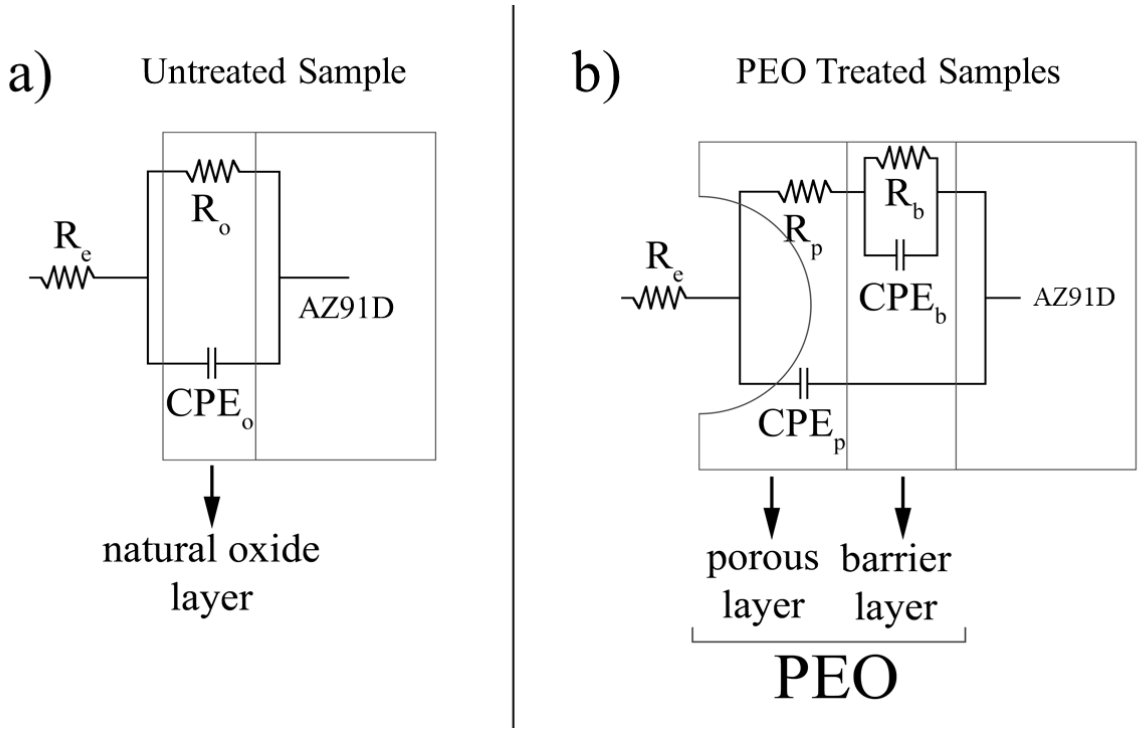

Fig.14 *– Equivalent circuits used to fit data of EIS tests: (a) Untreated sample (b)PEO-treated samples*

Considering the physical meaning of the different elements of the equivalent circuits in Fig. 14, R_e represents the resistance of the electrolyte, R_o and CPE_o represente the natural oxide layer formed on the untreated AZ91D, R_p and CPE_p represents the porous layer of PEO coating whereas R_b and CPE_b the barrier layer. CPE_i were used in the equivalent circuits instead of capacitances due to the fact that the measured capacitance is not ideal.

***Tab.6** – Results of the fitting of the experimental data from EIS tests with the equivalent circuits reported in Fig. 9*

Sample	R_S (Ω*cm^2)	R_P (Ω*cm^2)	R_o /R_B (Ω*cm^2)	Q_P (F*cm^{-2}* Hz^{1-n})	n_P	Q_B/Q_o (F*cm^{-2}* Hz^{1-n})	n_o/ n_B	χ^2
Untreated	44.2	-	375	-	-	2.1 x10^{-4}	0.88	4 x10^{-3}
PEO 1 min	31.3	204.3	1726	2.0 x10^{-6}	0.75	5.1 x10^{-6}	0.81	3 x10^{-3}
PEO 3 min	55.9	352.1	2654	6.6 x10^{-6}	0.85	6.4 x10^{-6}	0.66	2 x10^{-3}
PEO + SiC 1 min	40.2	196.4	1389	3.5 x10^{-6}	0.95	1.8 x10^{-6}	0.74	2 x10^{-3}
PEO + SiC 3 min	22.9	222.3	2122	2.0 x10^{-6}	0.96	4.2 x10^{-6}	0.57	2 x10^{-2}
PEO + G 1 min	21.4	300.1	1957	4.5 x10^{-7}	0.78	2.9 x10^{-5}	0.77	5 x10^{-4}
PEO + G 3 min	34.3	50.3	4199	3.6 x10^{-6}	0.62	4.3 x10^{-6}	0.52	1 x10^{-3}
PEO + SiC + G 1 min	38.9	295.4	1602	3.2 x10^{-6}	0.73	3.9 x10^{-5}	0.7	3 x10^{-5}
PEO + SiC + G 3 min	30.2	310.2	2397	8.6 x10^{-5}	0.55	9.2 x10^{-7}	0.73	2 x10^{-3}

The Nyquist plots and the data reported in Tab. 6 confirmed that all the PEO-treated samples are characterized by improved corrosion performance if compared to the untreated sample. In fact, the total polarization resistance, that can be qualitatively evaluated by the real part of the impedance at low frequencies, increased of about one order of magnitude passing from the untreated to the PEO-treated samples. Considering the PEO-treated samples, a clear trend in the corrosion properties with the addition of the particles and with the treatment time was observed. Every sample treated at 3 min showed improved corrosion performance by comparison with the corresponding one at 1 min. In fact, R_B increased from 1726 to 2654 Ω*cm^2 in the PEO samples, from 1389 to 2122 Ω*cm^2 in the PEO + SiC samples, from 1957 to 4199 Ω*cm^2 in the PEO + G samples and from 1602 to 2397 Ω*cm^2 in the PEO + SiC + G samples. This fact can be related to the previously reported microstructural observation: the samples obtained at 3 min are in fact characterized by a thicker protective layer, as evidenced in Fig. 2-3 and Tab.3. This produced an increase in the corrosion performance due to an increase in the barrier effect. The improvement in the corrosion resistance with the increase in the thickness of the coating, at least until these limits, is also in accordance with the literature [8].

The effect of the particles depended on particles nature. The addition of SiC particles produced a decrease in the corrosion performance. In fact, the values of R_B for the PEO + SiC sample at 1 and 3 min were lower than those of the corresponding PEO samples. This fact can be related to the conductive nature of the SiC particles that produced a reduction in the insulating properties of the film, decreasing the corrosion performances. This fact was in accordance with the literature, indicating that SiC generally did not produce improvement in the corrosion properties especially in the case of particles with micrometric size, as in this case. [19] The addition of borosilicate glass particles produced a totally different effect. Both the samples PEO +G (1 min and 3 min) were in fact characterized by increased values of polarization resistance by comparison with the corresponding PEO samples. In particular, the sample PEO + G obtained with 3 min of treatment time showed the best corrosion performance, characterized by a value of R_B of 4199 $\Omega*cm^2$. This behavior can be related to the rapid melting and solidification of the glass particles that induced pore sealing, as evidenced by the SEM micrographs of Fig. 2 and Fig. 3. When the pores are sealed the corrosion properties increased, as reported in literature with other types of sealing [45], and also in the only work that reports on the addition of glass particles in the electrolyte. [20] When a combination of SiC and borosilicate glass particles (SiC + G samples) is dispersed into the electrolyte and incorporated into the PEO layer, an intermediate behavior between PEO + SiC and PEO + G samples was recorded. In particular, the samples PEO + SiC + G showed substantially the same polarization resistance, by comparison with the standard PEO samples.

3.3 Tribological behaviour

The results of tribological tests, in terms of steady-state COF and maximum wear depth measured on PEO coated sliders, are shown in Fig. 15. It is worth noting that wear depth was considered as a more reliable index than wear volume (calculated from wear scar width data according to ASTM G77), because all the wear scars on PEO layers which survived the test were extremely non-homogeneous in terms of width and partly covered by transfer layers (Fig. 17).

Representative plot of COF and system wear, dynamically acquired during tribological tests, are reported in Fig. 16 as a function of sliding distance. As showed by Fig. 15a, the steady-state COF of 1 min PEO, PEO + SiC, PEO + G were comparable (~ 0.6). On the other hand, 1 min PEO + SiC + G showed a slighlty lower COF (~0.4), presumably due to its better surface quality. The increase of treatment time from 1 to 3 min did not affect the COF of PEO coating. In case of particles addition, for PEO coatings containing glass (PEO + G and PEO + SiC + G), the 3 min treatment succeeded in reducing the COF, while for 3 min PEO+SiC a marked increase in the COF was recorded. The COF

increase can be explained by recalling that friction force is defined by the sum of two different contributions: the adhesive one and the abrasive one. The presence of hard and angular SiC particles increases the abrasive component, that is also linearly dependent on the attack angle, fairly high in case of angular particles [46]. The COF increase for the 3 min PEO+SiC is therefore related to the corresponding increase in the surface roughness, shown by Fig. 10. In fact, a high surfce roughness also increases the two-body abrasive interaction occuring in correspondence of hard asperities The effect of particles addition is also shown by the dynamic plots in Fig.16. After the run-in stage, the PEO and PEO + SiC + G at both 1 and 3 min treatments exhibited an almost stable COF, but the same was not observed in case of PEO + SiC and PEO + G. 1 and 3 min PEO + SiC coating showed an increasing COF with increasing sliding distance, related to the enhanced the abrasive component of the COF. The overall increase of the abrasive component of the COF due to SiC particles was also responsible for the highest steady-state COF exhibited by 3 min PEO + SiC (Fig.15a). Conversely, the beneficial effect of the borosilicate glass in combination of SiC particles that, as already discussed, succeeded in reducing both surface roughness and scatter in the Lc3 load, positively influenced also the dry sliding tests. In fact, the COF of PEO + SiC + G, at both 1 and 3 min treatment time, remained low, as the sealing effect of glass probably compensated for the abrasive action of SiC particles.

The PEO + G 1 min treatment showed a COF decrease (starting already before 200 m) associated to a remarkable system wear increase (indicating material removal, as explained in section 2.4) shown in Fig. 16. This result, as discussed later, is due to the coating being worn out and the substrate being involved in the contact, as highlighted also by the highest wear depth in Fig.15b. The same coating obtained with the 3 minutes treatment time, instead, showed a stable COF. The absence of friction and wear transitions in this case is probably due to the increased thickness of the coating, which allowed it to withstand the test without being worn out.

As regards slider wear depths (Fig.15b), the 3 min glass-containing coatings (PEO+G and PEO+SiC + G) exibited increased wear resistance by comparison to 1 min ones, due to the beneficial influence of increased PEO layer thickness and adhesion. All the 3 min coatings showed comparable wear depths, always lower than coatings thickness (Tab. 3). In the case of the 1 min coatings, PEO + G showed the highest wear depth, being totally removed during the test, as previously mentioned and as showed also SEM analyses of wear tracks reported in Fig.17. In this case, at the end of the test only severe ploughing of the bare substrate was observed due to complete removal of the coating. The wear resistance of PEO + G improved by addition of SiC, allowing PEO + SiC + G coating to withstand the sliding test at both tested treatment times (1 and 3 min). Alternatively, wear resistance of PEO + G can be improved by the increased thickness attained at 3 min treatment time, which also lead to a slight wear resistance improvement by comparison to the PEO layer without added particles.

For all PEO coatings who survived the dry sliding tests, a mild trib-oxidative wear regime was observed, with a Fe-O based transfer layer from the steel countermaterial covering the wear tracks on the PEO-treated sliders (SEM images and corresponding EDS data in the supplementary material, Fig. S2). These transfer layers, typically observed on PEO coatings coupled with steel, may play a protective role, decreasing friction and reducing wear, and their formation vs consumption equilibria can be correlated to the dry sliding behaviour of the PEO layers [47-48].

In this case, for the PEO and PEO+SiC, the transfer layers thickness and homogeneity seems to decrease with increasing treatment time (as shown by the comparison of SEM images in the left column with those in the right column of Fig. 17), probably due to the increased surface roughness (Fig. 10) which led to and increased tendency of coating asperities to penetrate the transfer layer and make it less continuous, hence to slighty higher COF (Fig. 15a) and wear depth values (Fig. 15b).

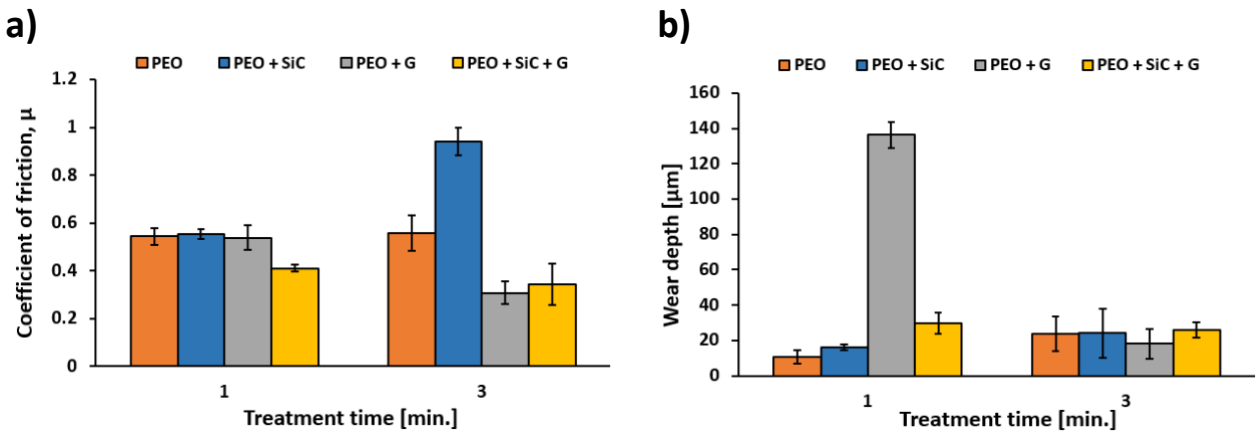

Fig.15 *– Dry sliding tests: a) COF vs treatment time, b) wear depth vs treatment time for the PEO treated samples: PEO, PEO + SiC, PEO + G and PEO + SiC + G*

Sample	Treatment time	
	1 min.	3 min.
PEO	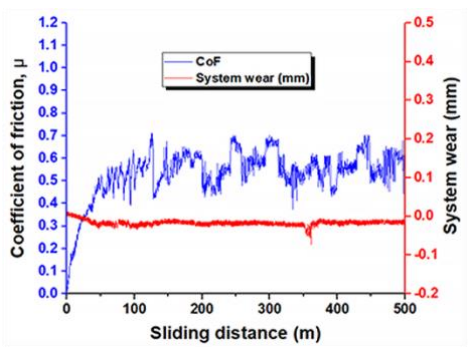	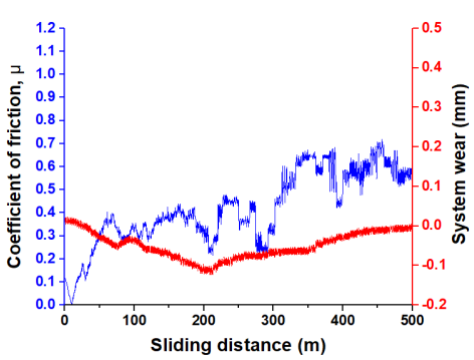

PEO + SiC	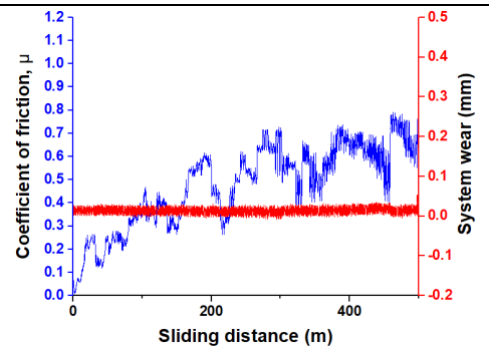	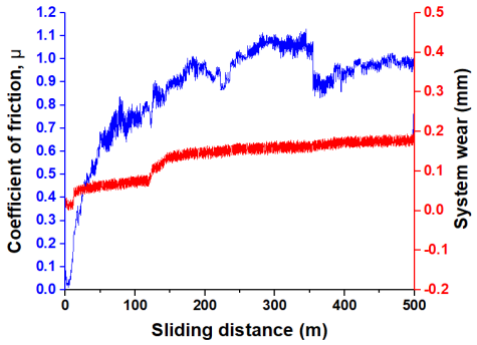
PEO + G	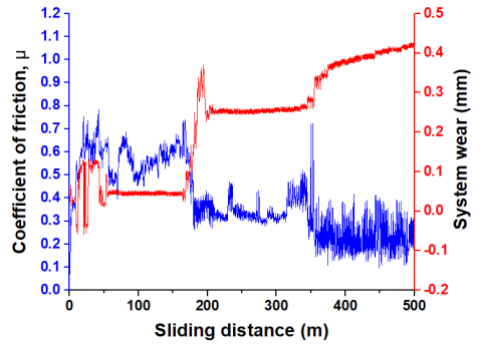	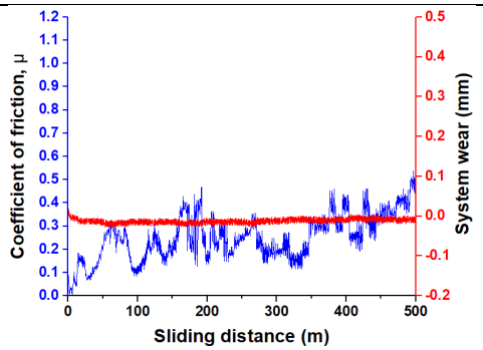
PEO + SiC + G	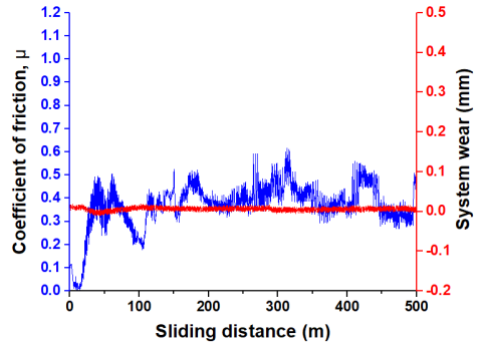	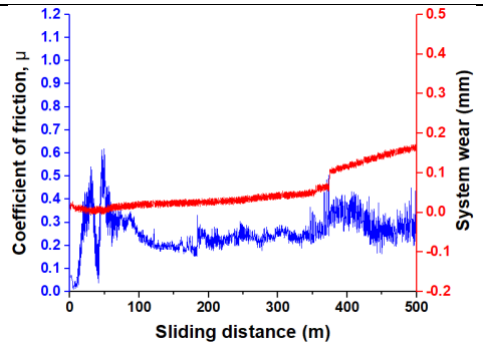

Fig.16 *– Dry sliding tests: representative dynamic COF and system wear as a function of the sliding distance for 1 and 3 min PEO treated samples*

Sample	1 min.	3 min.
PEO	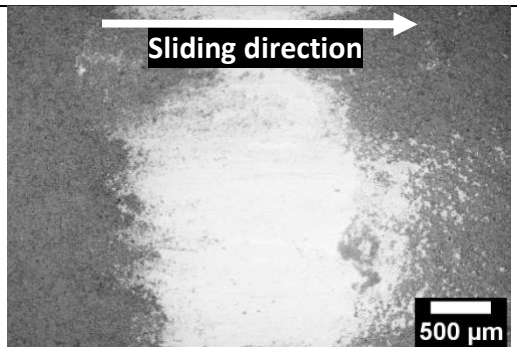	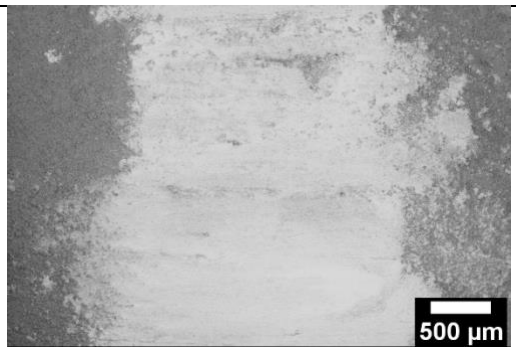

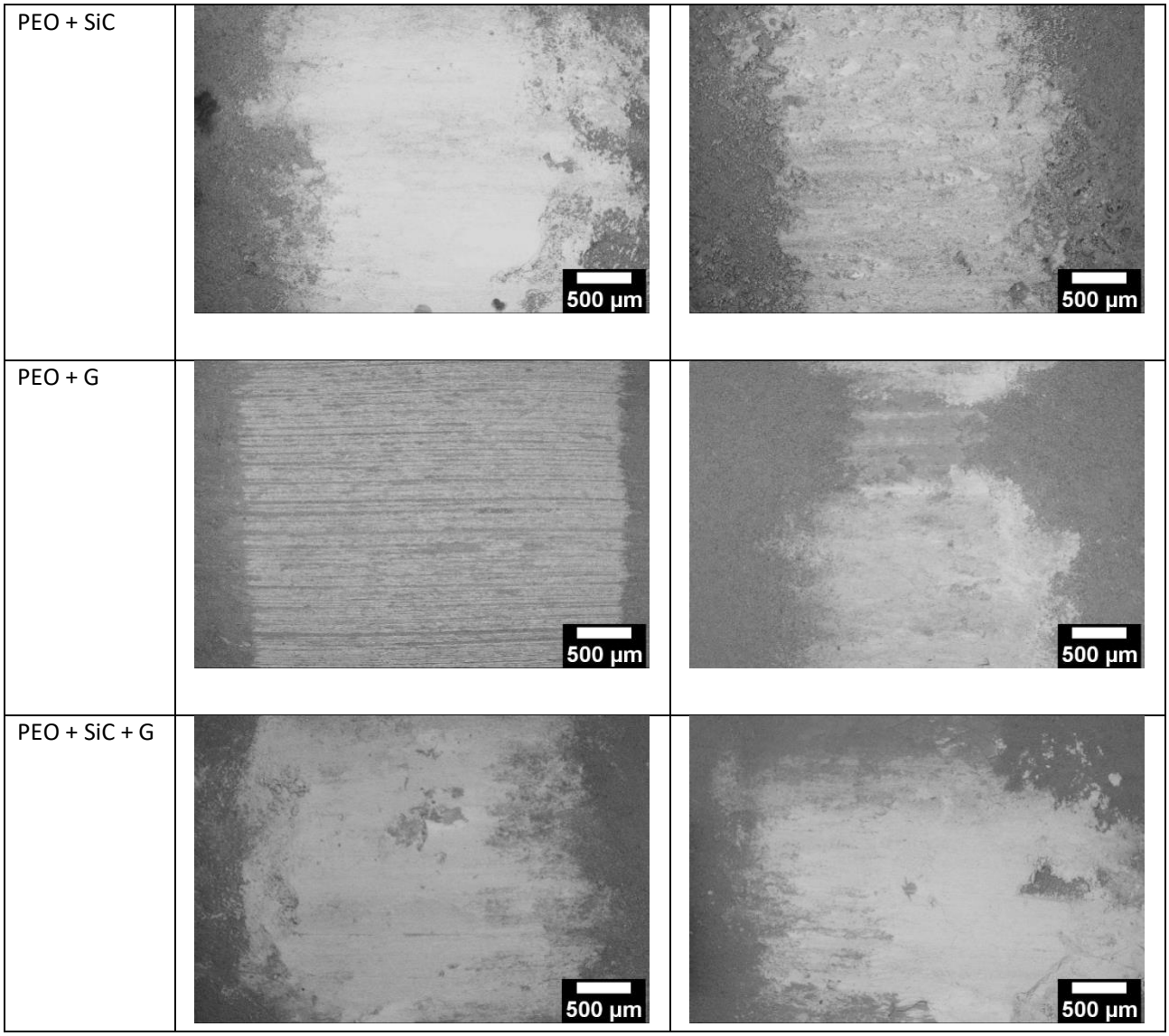

Fig.17 – *Representative SEM images of wear tracks on PEO treated samples after dry sliding tests*

4. Conclusions

Considering the production of PEO layers containing SiC and glass particles, the following conclusions can be drawn:

-Both SiC and borosilicate glass particles were successfully incorporated into PEO coatings that resulted mainly composed by $MgSiO_4$, SiO_2, MgO, MgOH, $Mg_3(PO_4)_2$ and Na_3PO_4. SiC particles entered into the PEO layer through inert incorporation, instead glass particles were melted and solidified during the treatment, producing an amorphous phase that sealed the pores. This different behavior was related to the different melting points of the compounds.

- The effect of the particles on the corrosion properties depended on particles nature. The addition of SiC particles produced a decrease in the corrosion properties, due the conductive nature of SiC, whereas the presence of the borosilicate glass particles produced an increase of the corrosion properties due to the sealing effect of the amorphous layer. The combination of both SiC and glass particles produced and intermediate behavior comparable to the one of the samples without particles addition.

-As far as the dry sliding behaviour is concerned, the addition of SiC alone increased the coefficient of friction without improving the wear resistance of PEO layer. The addition of glass particles alone improved both friction and wear only at 3 min treatment time, thanks to the improved roughness, thickness and adhesion of the PEO layer, leading to the lowest COF and wear depth values. The addition of both SiC and glass reduced friction and improved practical adhesion already after 1 min treatment (while the addition of glass alone led to complete wear of the coating), due to the beneficial combination of the sealing ability of glass and the load bearing capacity of SiC during the scratch test. However, the addition of SiC did not induce a significant increase of wear resistance in dry sliding tests, probably due to defects at the particle/coating interface, which also led to microhardness values lower than expected.

-Considering the corrosion and wear performance, the best combination of properties was obtained with the addition of glass particles for 3 min treatment time. In this way, both the corrosion and wear resistance were increased, without the detrimental effects of SiC on the corrosion properties and on the friction coefficient.

Acknowledgements

The Department of Chemical Sciences of the University of Padova is gratefully acknowledged for financial support and provision of XPS equipment. The authors would like to thank Prof. S. Gross (DiSC) for the helpful discussion.

Data availability

The raw/processed data required to reproduce these findings cannot be shared at this time as the data also forms part of an ongoing study

Conflict of interest statement

On behalf of all authors, the corresponding author states that there is no conflict of interest.

References

[1] R. O. Hussein and D. O. Northwood, Improving The Performance of Magnesium Alloys for Automotive Applications, WIT Transactions on The Built Environment. 137 (2014) 531-544.

[2] S. Housh, B. Mikucki, A. Stevenson, Selection and Application of Magnesium and Magnesium Alloys, in: ASM Handbook, Volume 2: Properties and Selection: Nonferrous Alloys and Special-Purpose Materials, ASM International, 1990, pp. 455-479.

[3] G.L. Song, Corrosion behavior of magnesium alloys and protection techniques, in: H. Dong (Ed.), Surface Engineering of Light Alloys, Woodhead Publishing Limited and CRC Press LLC, 2010, pp. 3–39.

[4] P.J. Blau, M. Walukas, Sliding friction and wear of magnesium alloy AZ91D produced by two different methods, Tribol. Int. 33 (2000) 573–579

[5] J.E. Gray, B. Luan, Protective coatings on magnesium and its alloys — a critical review, J. Alloy. Compd. 336 (2002) 88–113

[6] B. A. Shaw, R. C. Wolfe, Corrosion of Magnesium and Magnesium-Base Alloys, ASM Handbook, Volume 13B: Corrosion: Materials (S.D. Cramer, B.S. Covino, Jr., editors) p. 205-227

[7] C. Blawert, W. Dietzel, E. Ghali, G. Song, Anodizing Treatments for Magnesium Alloys and Their Effect on Corrosion Resistance in Various Environments, Adv. Eng. Mater. 8 (2006) 511-533.

[8] S. Sikdar, P.V. Menezes, R. Maccione, T. Jacob, P.L. Menezes, Plasma Electrolytic Oxidation (PEO) Process—Processing, Properties, and Applications, Nanomaterials. 11 (2021) 1375.

[9] X. Lu, M. Mohedano, C. Blawert, E. Matykina, R. Arrabal, K.U. Kainer, M. L. Zheludkevich, Plasma electrolytic oxidation coatings with particle additions – A review, Surf. Coat. Technol. 307 (2016) 1165-1182.

[10] M. O'Hara, S.C. Troughton, R. Francis, T.W. Clyne, The incorporation of particles suspended in the electrolyte into plasma electrolytic oxidation coatings on Ti and Al substrates, Surf. Coat. Technol. 385 (2020) 125354.

[11] R. Sola, L. Tonelli, P. Shashkov, T.H. Bogdanoff, C. Martini, Anodizing of AA6082-T5 by conventional and innovative treatments: Microstructural characterization and dry sliding behavior, Wear. 458–459 (2020) 203423.

[12] P. Cerchier, L. Pezzato, E. Moschin, L. B. Coelho, M. Olivier, I. Moro, M. Magrini, Antifouling properties of different Plasma Electrolytic Oxidation coatings on 7075 aluminium alloy, International Biodeterioration & Biodegradation.133 (2018) 70-78.

[13] L. Pezzato, P. Cerchier, K. Brunelli, A. Bartolozzi, R. Bertani, M, Dabalà, Plasma electrolytic oxidation coatings with fungicidal properties, Surf. Eng. 35 (2019) 325-333.

[14] X. Lu, S. P. Sah, N. Scharnagl, M. Störmer, M. Starykevich, M. Mohedano, C. Blawert, M.L. Zheludkevich, K.U. Kainer, Degradation behavior of PEO coating on AM50 magnesium alloy produced from electrolytes with clay particle addition, Surf. Coat. Technol. 269 (2015) 155-169.

[15] A. Fattah-alhosseini, R. Chaharmahali, K. Babaei, Effect of particles addition to solution of plasma electrolytic oxidation (PEO) on the properties of PEO coatings formed on magnesium and its alloys: A review, J. Magnes. Alloy. 8 (2020) 799-818.

[16] Y. Yang, Y. Liu, Effects of Current Density on the Microstructure and the Corrosion Resistance of Alumina Coatings Embedded with SiC Nano-particles Produced by Micro-arc Oxidation, J. Mater. Sci. Technol. 26 (2010) 1016-1020.

[17] L. Yu, J. Cao, Y. Cheng, An improvement of the wear and corrosion resistances of AZ31 magnesium alloy by plasma electrolytic oxidation in a silicate–hexametaphosphate electrolyte with the suspension of SiC nanoparticles, Surf. Coat. Technol. 276 (2015) 266-278.

[18] H. N. Vatan, R. Ebrahimi-kahrizsangi, M. Kasiri-asgarani, Structural, tribological and electrochemical behavior of SiC nanocomposite oxide coatings fabricated by plasma electrolytic oxidation (PEO) on AZ31 magnesium alloy, J. Alloy. Compd. 683 (2016) 241-255.

[19] X. Lu, C. Blawert, K.U. Kainer, T. Zhang, F. Wang, M. L. Zheludkevich, Influence of particle additions on corrosion and wear resistance of plasma electrolytic oxidation coatings on Mg alloy, Surf. Coat. Technol. 352 (2018) 1-14.

[20] M. Asgari, H. Daneshmand, G. Bratai Darband, A. Sabour Rouhaghdam, Single-stage production of glass sealed PEO composite coating on AZ31B, Surf. Interfaces. 21 (2020) 100712.

[21] L. Pezzato, R. Babbolin, P. Cerchier, M. Marigo, P. Dolcet, M. Dabalà, K. Brunelli, Sealing of PEO coated AZ91magnesium alloy using solutions containing neodymium, Corros. Sci. 173 (2020) 108741.

[22] M. P. Seah, D. S. Briggs, J. Practical Surface Analysis, Auger and X-ray Photoelectron Spectroscopy, 1st edition, Wiley, 1990.

[23] D. A. Shirley, High-resolution X-ray photoemission spectrum of the valence bands of gold, Phys. Rev. B. 5 (1972) 4709–4714.

[24] J. Chastain, R.C. King, J. Moulder, Handbook of X-RayPhotoelectron Spectroscopy: a Reference Book of Standard Spectra for Identification and Interpretation of XPS Data; Physical Electronics Division, Perkin-Elmer Corporation: Eden Prairie, MN, 1995

[25] X-ray Photoelectron Spectroscopy Database 20, Version 3.0, Gaithersburg.

[26] L. Kang, J. Gao, H.R. Xu, S.Q. Zhao, H. Chen, P.H. Wu, Epitaxial Mg_2SiO_4 thin films with a spinel structure grown on Si substrates, Journal of Crystal Growth. 297 (2006) 100–104.

[27] Y. Mori, A. Koshi, J. Liao, H. Asoh, and S. Ono, Characteristics and corrosion resistance of plasma electrolytic oxidation coatings on AZ31BMg alloy formed in phosphate—silicate mixture electrolytes, Corros. Sci. 88 (2014) 254–262.

[28] ISO 4288:1998, Geometric Product Specification (GPS) — Surface texture — Profile method: Rules and procedures for the assessment of surface texture, 1998

[29] ASTM G-77 - 17, Standard Test Method for Ranking Resistance of Materials to Sliding Wear Using Block-On-Ring Wear Test, 2017, https://doi.org/10.1520/G0077-17.

[30] Y. Gu, W. Xiong, C. Ning, J. Zhang, Residual Stresses in Microarc Oxidation Ceramic Coatings on Biocompatible AZ31 Magnesium Alloys, J. Mater. Eng. Perform. 21 (2011) 1–6.

[31] J.A. Curran, T.W. Clyne, Porosity in plasma electrolytic oxide coatings, Acta Materialia. 54 (2006) 1985-1993.

[32] G. Barati Darband, M. Aliofkhazraei, P. Hamghalam, N. Valizade, Plasma electrolytic oxidation of magnesium and its alloys: Mechanism, properties and applications, J. Magnes. Alloy. 5 (2017) 74-132.

[33] S. Wang, N. Si, Y. Xia, L. Liu, Influence of nano-SiC on microstructure and property of MAO coating formed on AZ91D magnesium alloy, Trans. Nonferrous Met. Soc. China. 25 (2015) 1926-1934.

[34] M. Mohedano, R. Arrabal, B. Mingo, A. Pardo, E. Matykina, Role of particle type and concentration on characteristics of PEO coatings on AM50 magnesium alloy, Surf. Coat. Technol. 334 (2018) 328-335.

[35] K.M. Lee, B.U. Lee, S.I. Yoon, E.S. Lee, B. Yoo, D.H. Shin, Evaluation of plasma temperature during plasma oxidation processing of AZ91 Mg alloy through analysis of the melting behavior of incorporated particles, Electrochimica Acta. 67 (2012) 6-11.

[36] L. Pezzato, V. Angelini, K. Brunelli, C. Martini, M. Dabalà, Tribological and corrosion behavior of PEO coatings with graphite nanoparticles on AZ91 and AZ80 magnesium alloys, Trans. Nonferrous Met. Soc. China 28 (2018) 259-272.

[37] A.G. Rakoch, E.P. Monakhova, Z.V. Khabibullina, M. Serdechnova, C. Blawert, M.L. Zheludkevich, A.A. Gladkova, Plasma electrolytic oxidation of AZ31 and AZ91 magnesium alloys: Comparison of coatings formation mechanism, J. Magnes. Alloy. 8 (2020) 587-600.

[38] Z.U. Rehman, B.H. Koo, Effect of $Na_2SiO_3 \cdot 5H_2O$ concentration on the microstructure and corrosion properties of two-step PEO coatings formed on AZ91 alloy, Surf. Coat. Technol. 317 (2017) 117-124.

[39] L. Pezzato, K. Brunelli, E. Napolitani, M. Magrini, M. Dabalà, Surface properties of AZ91 magnesium alloy after PEO treatment using molybdate salts and low current densities, Appl. Surf. Sci. 357 (2015) 1031-1039.

[40] M. Mohedano, X. Lu, E. Matykina, C. Blawert, R. Arrabal, M.L. Zheludkevich, Plasma Electrolytic Oxidation (PEO) of Metals and Alloys, Editor(s): Klaus Wandelt, Encyclopedia of Interfacial Chemistry, Elsevier, 2018, pp. 423-438.

[41] ISO 20502:2005, Fine Ceramics (advanced ceramics, advanced technical ceramics) - Determination of Adhesion of Ceramic Coatings by Scratch Testing, 2005.

[42] L. Tonelli, L. Pezzato, P. Dolcet, M. Dabalà, C. Martini, Effects of graphite nano-particle additions on dry sliding behaviour of plasma-electrolytic-oxidation-treated EV31A magnesium alloy against steel in air, Wear. 404–405 (2018) 122-132

[43] J.M. Wheeler, J.A. Curran, S. Shrestha, Microstructure and multi-scale mechanical behavior of hard anodized and plasma electrolytic oxidation (PEO) coatings on aluminum alloy 5052, Surf. Coat. Technol. 207(2012) 480-488

[44] Y.S. Huang, X.T. Zeng, I. Annergren, F.M. Liu, Development of electroless NiP–PTFE–SiC composite coating, Surf. Coat. Technol. 167 (2003) 207–211.

[45] B. Mingo, R. Arrabal, M. Mohedano, Y. Llamazares, E. Matykina, A. Yerokhin, A. Pardo, Influence of sealing post-treatments on the corrosion resistance of PEO coated AZ91 magnesium alloy, Appl. Surf. Sci. 433 (2018) 653-667.

[46] G. Straffellini, Friction and Wear, doi:10.1007/978-3-319-05894-8, ISNB: 978-3-319-05893-1

[47] G. Sabatini, L. Ceschini, C. Martini, J.A. Williams, I.M. Hutchings, Improving sliding and abrasive wear behaviour of cast A356 and wrought AA7075 aluminium alloys by plasma electrolytic oxidation, Materials & Design. 31 (2010) 816-828.

[48] C. Martini, L. Ceschini, F. Tarterini, J.M. Paillard, J.A. Curran, PEO layers obtained from mixed aluminate–phosphate baths on Ti–6Al–4V: Dry sliding behaviour and influence of a PTFE topcoat, Wear. 269 (2010) 747-756.